

Surfactants Control Optical Trapping near a Glass Wall

Jeonghyeon Kim and Olivier J. F. Martin*



Cite This: *J. Phys. Chem. C* 2022, 126, 378–386



Read Online

ACCESS |



Metrics & More

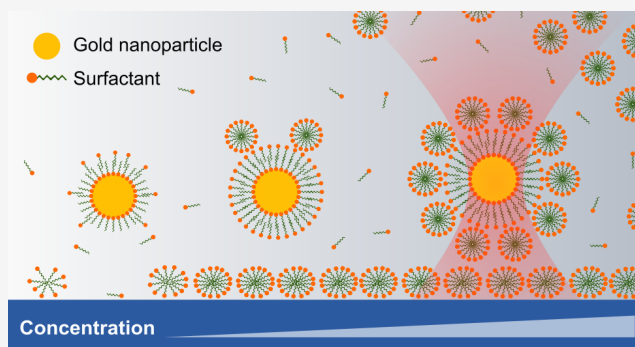


Article Recommendations



Supporting Information

ABSTRACT: Beyond their original capability to grab and hold tiny objects, optical tweezers have emerged as a powerful tool to investigate fundamental physics at microscopic scales. A precise characterization of the optical trap is one of the key requirements in such applications. A typical trapping system often involves a colloidal particle, stabilized in a fluid as an optical probe. Surfactants are commonly added to provide colloidal stability, but their incidental effects on the tweezer–particle interactions have been overlooked despite their prevalent use. Here, we study the interplay among the tweezer, the particle, and the surfactants adsorbed on the interfaces, including a nearby glass wall. In trapped particles' motion analysis, we find that the surfactants can affect the motion of the particle through the interactions between them. We discuss the effect of the surfactants' assembly structures on the particles' statistical behaviors. In particular, we investigate the thermal effect on the particle surroundings induced by the optically heated particle by analyzing the difference between metallic and dielectric probes. Our results explain how, under nanoscale confinement, the adsorbed surfactants can affect the particle behavior in an optical trap and propose a possible strategy of using an optically heated particle for localized surface modulation.



INTRODUCTION

Since the 1970s, when Ashkin first demonstrated the utilization of radiation pressure for optical manipulations,^{1–4} optical tweezers have been successfully applied to various fields,^{5–7} notably in biology, to manipulate small viruses and bacteria^{8–10} or to observe some of the smallest forces in life produced by motor proteins.^{11,12} Apart from biological applications, they have provided an ideal test bench to study fundamental physics in colloid and interface sciences,¹³ ranging from hydrodynamics^{14,15} to thermodynamics.^{16–18}

Colloidal micro- or nanoparticles are the optical probes of choice to study physical phenomena at the nanoscale with optical tweezers.^{14–18} By tracking a particle, we can characterize its immediate surrounding at the nanoscale.^{13,15,19} However, this also requires precise characterization of the optical trap itself²⁰ and an understanding of the dynamics and interactions of particles suspensions in fluids.

Among a variety of soft materials that constitute the environment of a probe in an optical trap, ionic surfactants play a fundamental role in colloidal suspensions. They develop charged layers on surfaces and prevent aggregation by providing electrostatic repulsion.^{21,22} Consequently, trapping experiments with colloidal nanoparticles inherently involve the effects of surfactants. In particular, these effects can have a substantial impact under nanoscale confinement, where the surface area to volume ratio increases significantly. However, despite their ubiquitous role in optical trapping, the many-sided effects of surfactants have not yet received significant consideration in trap

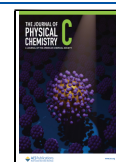
characterization. It is only recently that surfactants have drawn researchers' attention, particularly, to their thermoelectric^{23,24} or thermophilic/thermophobic influences²⁵ on plasmonic optical traps. These studies reported the role of surfactants in optical trapping, but they also limited their discussions to the thermal response of surfactants in the bulk medium;^{23,25} the effects of surfactants on surfaces still remain elusive.

Here, we describe the primary effect of surfactants on the optical traps, particularly at the vicinity of surfaces. For this, we analyze the motion of an optically trapped particle near a glass wall using high-speed video microscopy.^{26–28} We construct the simplest possible environment, consisting of a surfactant solution at various concentrations and a glass chamber to contain fluids. We study cetyltrimethylammonium chloride (CTAC) as an example of cationic surfactant and a gold nanoparticle as an optical probe. The gold nanoparticles have unique optical properties, such as large scattering and absorption cross sections, making them outstanding imaging tracers^{29,30} and nanoscale thermal probes.^{31–33} Along with classical video analysis,²⁶ we examine the zeta potentials of the gold nanoparticles as well as their hydrodynamic sizes, which change

Received: October 14, 2021

Revised: November 30, 2021

Published: December 29, 2021



as a consequence of the surfactant structures adsorbed on the surfaces. Based on this information, we propose a plausible model to explain the influence of the surfactants, particularly those at the interfaces, on the trapped particles' behaviors. We also hypothesize that the optical heating of the particles by the trapping laser can perturb the surfactant assemblies, which can act back on the particle's motion. Controlled experiments with polystyrene beads as a nonthermal probe are performed to support this interpretation.

METHODS

Materials. Cetyltrimethylammonium chloride (CTAC) was obtained from Sigma-Aldrich in solution (25 wt % in H₂O). The CTAC solution was diluted with distilled water to reach desired concentrations. Gold nanoparticles with a 150 nm diameter, stabilized suspension in citrate buffer, were purchased from Sigma-Aldrich. Polystyrene (PS) beads (210 nm diameter), which have carboxyl (–COOH) coatings and contain fluorophores (Flash Red, absorption maximum at 660 nm, emission at 690 nm), were purchased from Bangs Laboratories, Inc. The nanoparticle suspensions were centrifuged and redispersed in the CTAC solution using a vortex mixer. We adjusted the particle concentration by diluting 1 part of the particle solution with 500 parts of the CTAC solution of the desired concentration (1000 parts for PS beads) to reduce the particle concentration sparse enough to ensure single-particle trapping.

Glass coverslips from Menzel Gläser (145 μm in thickness) and a double-sided adhesive spacer (120 μm thickness, Grace Bio-Laboratories SecureSeal imaging spacer) were used to build a microfluidic chamber. Glass coverslips were sonicated in acetone and isopropyl alcohol for 30 min each, before use.

Optical Measurements. The gold nanoparticles and fluorescent polystyrene beads in the microfluidic chamber were imaged using a commercial optical microscope (IX71, Olympus) equipped with a 60×, 1.45 NA, oil-immersion objective (PLAPON 60xO TIRFM, Olympus). Supporting Information Figure S1 provides an overview of the optical setup. The imaging system is essentially reflected dark-field microscopy. The samples were illuminated from below through the objective. The backward scattered light from the specimen was collected by the same objective lens, transmitted through a dark-field mirror. The dark-field mirror is a transparent plate with a small elliptical silvered mirror in the center, tilted at an angle of 45° to the optical path. The projection of this elliptical mirror onto the transverse plane is a circular light stop, which blocks the direct reflection of the light source and the trapping laser and transmits only the high-angle part of the scattering to form a dark-field image.³⁴ The sample stage incorporated a three-dimensional piezoelectric translation for the high precision control of the sample position.

Trapping Experiments. A 632.8 nm linearly polarized He–Ne laser was used for particle trapping. The power of the laser was controlled in front of the laser using a laser-line variable beamsplitter (VA5–633, Thorlabs) to have a power of 10 mW before the entrance pupil of a trapping objective. The laser beam was focused at the bottom of the microfluidic chamber using a 60×, 0.85 NA, air objective lens to trap the particle close to the water–glass interface. The beam was not expanded and therefore underfilled the objective's entrance pupil. The resulting low numerical aperture produced a large radiation pressure toward the substrate, bringing particles close to the bottom of the microfluidic chamber. A stable optical trap was

formed by balancing the radiation pressure and the electrostatic repulsion between the positively charged particles and the positively charged glass wall. The trapping objective was mounted on another piezoelectric stage for precise adjustment of the optical trap position.

Particle Tracking. The movement of a trapped particle was recorded by a CMOS camera (CM3-U3-5055C-CS, FLIR) at a frame rate of 346 frames per second. An additional short pass filter with a 600 nm cutoff wavelength was included in the imaging path to cut the laser light scattered by the particle. The position of a particle was determined using a Python package, Trackpy,³⁵ which uses the feature-finding and linking algorithms developed by Crocker and Grier.²⁶ All trajectories for trapped particles were collected for at least 20 s (10 s for PS beads due to relatively weak axial trapping stiffness), which corresponds to ~7000 frames. We provide an open access data set for the particle recordings and the corresponding trajectories and MSD analysis in ref 36.

Colloidal Properties. The characteristics of colloidal particles in surfactant solutions, including their hydrodynamic sizes and zeta (ζ) potentials, were measured using dynamic light scattering (Zetasizer Nano ZS, Malvern Panalytical). The conductivities of the samples were also determined during the ζ potential measurements. For optimal measurements, the particle concentration was adjusted according to the stock particle concentration. Supporting Information Figure S2 shows the effect of gold colloid concentration on the ζ measurements. The average ζ potentials remain independent of dilution factors, but the lowest particle concentration is subject to large variance due to a low signal-to-noise ratio. The dilution factors (10 times for gold nanoparticles and 100 times for PS beads) were selected accordingly.

RESULTS AND DISCUSSION

Mean Squared Displacement. We examined an optically trapped particle's statistical behavior as a function of CTAC concentration by analyzing its mean squared displacement (MSD). The MSD at time lag τ is defined as

$$\text{MSD}(\tau) \equiv \langle [x(t + \tau) - x(t)]^2 \rangle \quad (1)$$

where $x(t)$ is the position of the particle as a function of time t , i.e., the particle trajectory. The MSD can be thought of as an area explored by a particle in a given time lag τ .

The optically trapped particle is modeled as a damped harmonic oscillator in a heat bath.³⁷ To keep a constant temperature, we fixed the size and material of the particles (gold and 150 nm in diameter) and the incident laser power (10 mW before the trapping objective). These three parameters determine the amount of optical heating by the laser.^{38,39} Supporting Information Figure S3 shows the measured absorbance spectrum of the 150 nm gold colloid; this particular colloid was carefully chosen to have its highest absorbance at the trapping laser's wavelength so that it not only acts as an optical probe but also serves as a localized heat source.

Based on the constant temperature assumption, we can describe the motion of a damped harmonic oscillator in one dimension with the Langevin equation⁴⁰

$$m\ddot{x}(t) + \gamma\dot{x}(t) + \kappa x(t) = F_{\text{therm}}(t) \quad (2)$$

where m is its inertial mass, γ is its friction (drag) coefficient, κ is the spring constant of the optical trap, and F_{therm} is the random thermal force acting on the trapped particle. On time scales

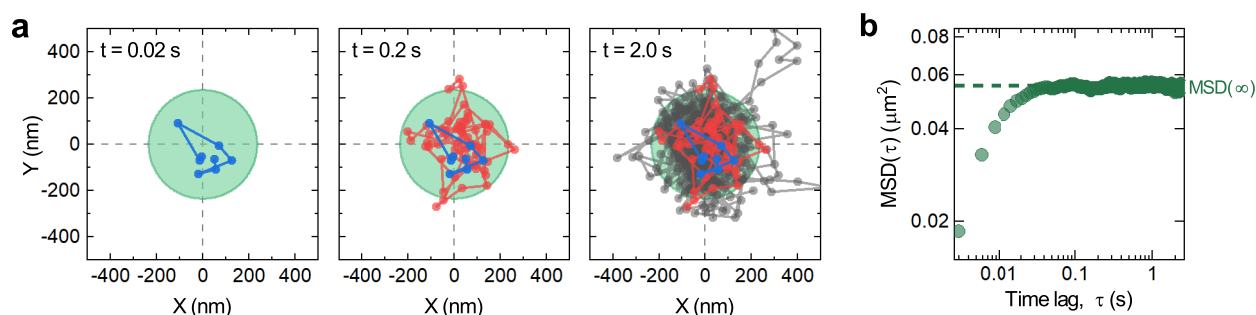


Figure 1. Particle trajectory in an optical trap and its mean squared displacement (MSD). (a) Example trajectories of a trapped particle at three different time scales (0.1 mM CTAC). The green circle has an area the same as the $\text{MSD}(\tau \rightarrow \infty)$, which indicates the area over which the particle is confined over a long time scale. (b) Double-logarithmic plot of the MSD calculated from the trajectory shown in a. The value of $\text{MSD}(\tau \rightarrow \infty)$ is indicated as the dashed horizontal line.

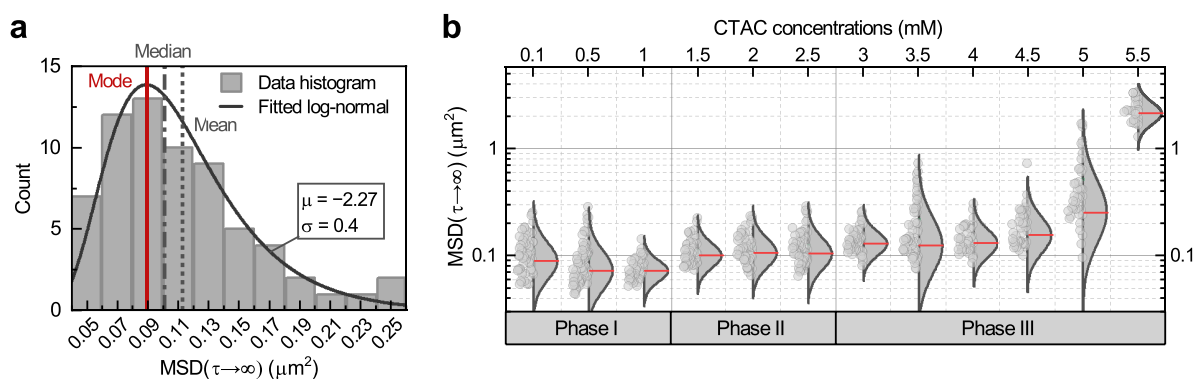


Figure 2. Statistical distribution of MSDs for different surfactant concentrations. (a) A typical example $\text{MSD}(\tau \rightarrow \infty)$ histogram for a total of 66 measurements at 0.1 mM CTAC. A log-normal distribution is fitted to the data histogram to approximate the skewed data distribution and to calculate the mode of the statistical population. (b) Semilogarithmic plot summarizing all the $\text{MSD}(\infty)$ as a function of bulk CTAC concentration. For each concentration, at least 30 trajectories are analyzed for the log-normal distribution fit. The red solid bars represent the mode values of each distribution.

longer than a few microseconds, the inertial term, $m\ddot{x}(t)$, becomes negligible in aqueous media due to the low Reynolds number.⁴¹ The reduced Langevin equation without the inertial term can be solved for MSD ,³⁷ which is

$$\text{MSD}(\tau) = \frac{2k_{\text{B}}T}{\kappa}(1 - e^{-\tau\kappa/\gamma}) \quad (3)$$

where k_{B} is the Boltzmann constant and T is the temperature.

Figure 1a shows an example of three successive trajectories for an optically trapped gold nanoparticle at different time scales. It visualizes the temporal evolution of the two-dimensional position fluctuations, $(X(t), Y(t))$, at increasing time intervals (0.02, 0.2, and 2.0 s). Figure 1b shows the MSD calculated from this trajectory. When the time lag τ becomes long enough, typically longer than 0.1 s in our experiments, the MSD reaches a plateau; we call it $\text{MSD}(\tau \rightarrow \infty)$ or simply $\text{MSD}(\infty)$, which is closely related to the area in which the particle's motion is confined by the restoring optical force. This area is shown as a green circle in Figure 1a. Eq 3 tells us that among the three variables that determine the $\text{MSD}(\tau)$, only the temperature T and the trapping stiffness κ decide the value of $\text{MSD}(\tau \rightarrow \infty)$, not the friction coefficient γ ; the value of γ affects the slope of the linear dependence on τ at short time scales (Figure 1b).

We have analyzed at least 30 trajectories for each concentration to obtain a distribution of $\text{MSD}(\tau \rightarrow \infty)$. An example distribution at 0.1 mM CTAC is plotted as a histogram in Figure 2a, which consists of 66 measurements. Interestingly, it reveals that the data set has a skewed distribution rather than a symmetric one. One possible explanation for this is the particle

size distribution, which is well-known to follow the log-normal distribution. Supporting Information Figure S4a shows the measured size distribution of the colloids used in this study, which is also well-approximated with a log-normal. The relationship between the size distribution and that of $\text{MSD}(\infty)$ can be inferred from eq 3, where $\text{MSD}(\tau)$ converges to $\frac{2k_{\text{B}}T}{\kappa}$ with $\tau \rightarrow \infty$. Since the trapping laser power was fixed for all the measurements, the stiffness κ can be assumed to be constant. Only the temperature T may vary with the size variance, as does the absorption by the particle. Figure S4b in the Supporting Information shows the Mie calculation for the absorption cross section with increasing particle size; a larger particle tends to have a larger absorption cross section, raise the temperature T , and therefore have a greater value for $\text{MSD}(\infty)$.

Such an asymmetric distribution appears for all the examined CTAC concentrations. We made a total of 651 measurements, i.e., 55 measurements on average for each concentration. We fitted each data set with a log-normal to observe the underlying trends for varying surfactant concentrations. The mode of the data set was also calculated from the log-normal fit as a statistical representative value (e.g., the red solid vertical line in Figure 2a). Figure 2b summarizes the results as a function of CTAC concentration. For each concentration, the data points are drawn on the left half, and the log-normal fit is drawn on the right half with the mode highlighted as the red horizontal bar. These mode values reveal that the different amounts of surfactants can strengthen or weaken the optical trap. We grouped the results into three categories (Phase I, II, and III)

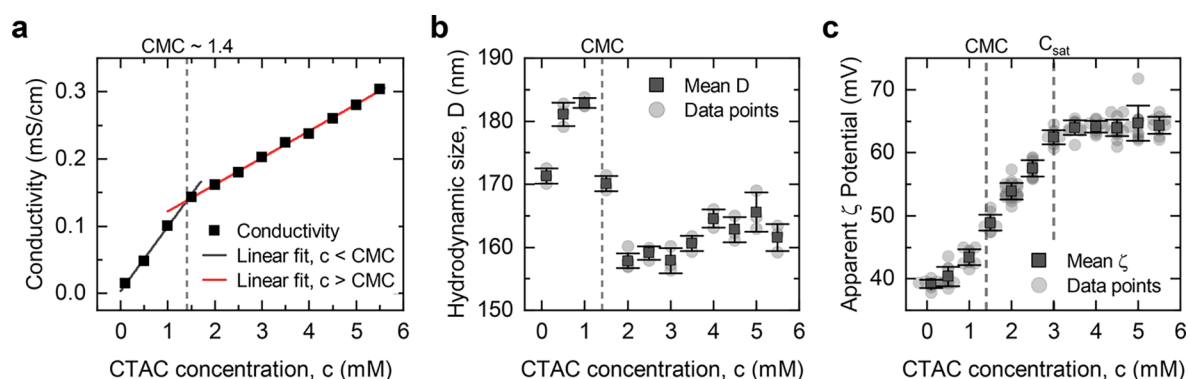


Figure 3. Critical micelle concentration (CMC) and colloid characteristics. (a) Conductivity of the bulk nanoparticle–surfactant solution and its piecewise linear fit to determine the CMC. (b) Hydrodynamic size and (c) zeta (ζ) potential of the colloidal gold nanoparticles as a function of CTAC concentration.

based on the trends discovered by the mode values. We will elaborate on each category and a plausible role of the surfactant in the following section.

Effect of Adsorbed Surfactants. CTAC surfactants adsorb on the glass and gold nanoparticle surfaces.^{42–44} On the glass surface, they form centrosymmetric aggregates, termed admicelles, which resemble micelles in the bulk solution.^{45,46} The formation of admicelles appears early in the adsorption process, at concentrations below the bulk critical micellar concentration (CMC).^{45,46} Tyrode et al.⁴⁶ performed a detailed study on the adsorption of cetyltrimethylammonium bromide (CTAB, the corresponding bromide salt of CTAC) on silica, and we refer to this paper for a detailed description of the adsorption process.

On the other hand, CTA⁺ molecules form a bilayer structure on the gold surfaces.⁴² A recent study by Li et al.⁴⁷ proposed an insightful mechanism for the assembly structure of CTA⁺ molecules on citrate-capped gold colloids, which varies not only with CTAB concentration but also with the ratio of CTAB molecules to gold nanoparticles.

We adapted these two studies by Tyrode et al.⁴⁶ and Li et al.⁴⁷ to understand how the CTA⁺ molecules adsorb and form assemblies on the different interfaces in our trapping system. (Although they studied CTAB instead of CTAC, both surfactants have cetyltrimethylammonium cations (CTA⁺) in common, and we assume that the effect of the halide counterions (Br[−] or Cl[−]) is not significant in this study where we consider the low concentration range at which both of CTAB and CTAC form similar aggregates.⁴⁸) Together with our measurements of the CMC, the particles' zeta (ζ) potentials, and their hydrodynamic size variation, we will provide a plausible interpretation of the relationship between the surfactant structures and the trapped particles' behaviors.

We first measured the conductivity of the gold colloid–surfactant solution as a function of CTAC concentration to determine the CMC in bulk. The CMC was determined as 1.4 mM by finding the intersection of two straight lines that were fitted into the conductivity/concentration data above and below the CMC^{49,50} (Figure 3a). This value of 1.4 mM is higher than the values reported in the literature (1.0 to 1.1 mM)^{44,51} possibly due to two factors: First, the bulk solution is a mixture of surfactants, gold nanoparticles, and water; the surfactants adsorb on the particles' surfaces, which effectively reduces the bulk concentration and thus shifts the apparent CMC to a slightly higher value. The second factor is related to the solution preparation step. We prepared the colloid and surfactant mixture

by centrifuging the gold colloids, carefully removing the supernatant, and redispersing the residue in the target CTAC solution. Since we cannot completely remove the supernatant, about 5% of the original buffer remains in the residue and dilutes the surfactant concentration. For these reasons, we found a slightly higher value for the CMC of the colloid–surfactant mixture, which will be used as the value for CMC throughout the discussion.

Figure 3b,c shows the hydrodynamic size and ζ potential of the gold colloids, which change as a function of CTAC concentration. When combined, these different measurements give valuable information about the surfactant structures on the particles' surfaces. According to the study by Li et al.,⁴⁷ the CTA⁺ cations form assembly structures on colloidal surfaces in the following order: incomplete monolayer → complete monolayer → imperfect bilayer → perfect bilayer → (perfect bilayer + micelles). The hydrodynamic size (171 nm) and ζ potential (39 mV) at the lowest CTAC concentration in Figure 3b,c imply that the surfactant molecules form at least imperfect bilayer structures on gold nanoparticle surfaces, whose charge was originally negative due to the citrate ions and became positive with the adsorption of the positively charged CTA⁺ cations. If the particles had not reached the imperfect bilayer state, remaining either in the state of the incomplete monolayer or complete monolayer (i.e., the hydrocarbon tail groups of the CTA⁺ molecules exposed to the bulk solution), they would have aggregated due to the hydrophobic effect among particles.⁴⁷ Since the size distribution shows a unimodal distribution with an average size of 171 nm (Supporting Information Figure S4a), it indicates no aggregate, and the CTA⁺ cations must form at least an imperfect bilayer assembly. These imperfect bilayers develop into perfect bilayers with increasing CTAC concentration, supported by the growing hydrodynamic size and ζ potential up to the CMC.

The glass–water interface also experiences a drastic change from the lowest concentration up to the CMC.⁴⁶ In this region, the surface coverage with admicelles rapidly increases and reaches its maximum above the CMC.⁴⁶ This type of adsorption behavior has been reported in the literature for various surfactant–substrate combinations^{45,46,52} and also extensively reviewed by Atkin et al.⁴⁴ Therefore, we assume that this general adsorption model also works for our glass–CTAC solution system.

Combining the observation for the gold nanoparticles and the assumption for the glass–solution interface in this concentration range below the CMC, we can expect increasing electrostatic

repulsion between the particle and the surface with the gradual adsorption of CTA⁺ molecules on both surfaces. This repulsive force can elevate the equilibrium position of the particle above the surface and thus can decrease the hydrodynamic drag⁵³ following Faxén's law.⁵⁴ However, in Supporting Information Figure S5, we calculated the drag coefficient γ by fitting the measured MSDs with eq 3 and found that the γ values remain similar over the whole concentration range. They do not show any close correlation with the ζ potentials of the particles nor with the surface coverage of the glass substrate. One possible explanation is that the radiation pressure by the optical tweezer dominates over the electrostatic repulsion and keeps pushing the particle close to the glass wall. Therefore, we can assume that the particle's axial position remains similar across the whole concentration range used in this study.

With this understanding, we construct a model for the lowest concentration range below the CMC to interpret the trapped particles' behaviors in Phase I (Figure 2b). In Phase I, the mode of the MSD(∞) distribution decreases, and the distribution itself is narrowing. Since $\text{MSD}(\tau \rightarrow \infty) = \frac{2k_B T}{\kappa}$ from eq 3, the decrease in MSD(∞) implies an increase in the trapping stiffness κ under the assumption of a constant average temperature. Based on the idea that the particle surface has an incomplete bilayer and the glass surface has yet to be fully covered below the CMC, we can hypothesize that these molecules are partly mobile, and they can rearrange themselves when the particle sits on the glass wall. This rearrangement then forms an additional lateral trapping potential, and the particle's MSD(∞) decreases as a consequence. This decreasing trend for the MSD(∞) can be understood by the fact that denser admicelles result in a deeper and narrower potential well.

Two driving forces can be proposed for the mobility and rearrangement: (1) the electrostatic repulsion between the particle and the surface admicelles and (2) the increased temperature around the particle by laser heating.^{32,55} In general, admicelles are mobile, and they can migrate over the surface without leaving the surface completely, which requires much less energy than desorption.⁵⁶ Around the optically trapped and heated nanoparticle, there is sufficient energy for the admicelles to diffuse over the surface, since the local temperature of an optically trapped gold nanoparticle can easily reach up to 100 °C even at moderate laser powers.^{38,39} The electrostatic repulsion can drive the micelles away from where the particle rests.

Once being settled around the trapped particle, these micelles can form an additional trapping potential, as we hypothesized based on the observed decreasing trend in MSD(∞) in Phase I. First, we estimated the magnitude of the interaction force between the particle and the micelle with the DLVO theory (Supporting Information Figure S6 and Section 6 for more details). The maximum magnitude of the repulsive force was ~ 0.46 pN, and it decreased exponentially with separation distance, h . For instance, at $h = 30$ nm, the force is repulsive and has a magnitude of 0.04 pN; a fraction of this force (i.e., a projection onto the lateral surface) contributes to the particle trapping. On the other hand, the optical force induced by the trapping laser also falls into similar magnitudes. The trapping stiffness of the optical trap at 0.1 mM CTAC (where the effects from admicelles are assumed to be minimal) is calculated as 1.13×10^{-7} N/m, using eq 3 with an estimated temperature of 366 K (Supporting Information Section 5 for more details). At around 170 nm displacement from the trap center, the same as the radius of the MSD(∞) shown in Figure 2a, the force is estimated

as 0.02 pN toward the trap center. The similarities in force magnitudes between the optical tweezer and admicelle/particle interaction imply that the electrostatic interaction between the admicelle and the particle is significant enough to influence the optical trap and thus the particle motion.

In the next phase of the MSD(∞), Phase II in Figure 2b, the distribution and its mode show a step-like increase above the CMC and then stagnate up to 2.5 mM. This transition should also be related to the change in the surfactant structure. Returning to Figure 3b, we find an abrupt decrease in the hydrodynamic size at 1.5 mM. Such an abrupt change indicates the involvement of a new species, which has a higher electrical charge than that of a single CTA⁺ molecule and thus more efficiently screens the particle's surface charge, making the electrical double layer thinner: the advent of micelles. The plummeting hydrodynamic size and the steeper rise in the ζ potential in Figure 3b,c substantiate together the existence of micelles in the particles' outer layers. Therefore, we estimate that the bilayer on the particle surface is almost complete at the end of Phase I, and the micelles in the bulk start to become associated with the particle in the beginning of Phase II.

These micelles at the particle–liquid interface apparently do not affect the MSD(∞), as its distribution stagnates throughout the three concentrations in Phase II. A plausible explanation is that these micelles are also mobile around the particle and rearrange themselves, similar to the previous assumption in Phase I. The step-like increase in the MSD(∞) can be explained by the fully occupied glass–liquid interface above the CMC. The admicelles are now closely packed and have lost their mobility. The previously mentioned effect of additional trapping potential created by the rearranged admicelles will disappear, which will raise the MSD(∞) values.

The final concentration region, Phase III in Figure 2b, features another step-like increase and exponential growth of MSD(∞). The second jump between 2.5 and 3 mM can be attributed to the complete saturation of the particle surface with micelles, similar to the first jump associated with the full coverage of the glass substrate. The plateau of the ζ potentials in Figure 3c supports the saturated adsorption on the particle surface. Since both the glass and particle surfaces are fully saturated at this stage, the adsorbed structures on the interfaces remain the same. The only variation with the increased concentration is the number of micelles in the bulk solution. The exponential growth in the MSD(∞) in Phase III indicates that the bulk micelles disturb stable trapping, and video investigations (Supplementary Video 1) also show impeded particle movements.

A recent study by Jiang et al.²⁵ provides a convincing explanation of this phenomenon. They studied the role of surfactants in plasmonic trapping and described that the surfactants in bulk could alter a trapped object's thermal response, making it thermophilic or thermophobic depending on the type of surfactants. Another study by Lin et al.²³ also reported a similar effect based on a nonuniform surfactant distribution in bulk upon a temperature gradient. In particular, they discovered that CTAC makes gold nanoparticles thermophilic driven by a surfactant-induced thermoelectric field, which enhanced the trapping stiffness of their thermoplasmonic trap 2–3 orders of magnitude higher than that of optical tweezers.²³ However, in our system, the heat source is the trapped particle itself, whose position and concomitant temperature gradient constantly fluctuate. Therefore, even if the CTAC makes the gold nanoparticle thermophilic, the self-induced thermoelectric field can disturb the optical trap.

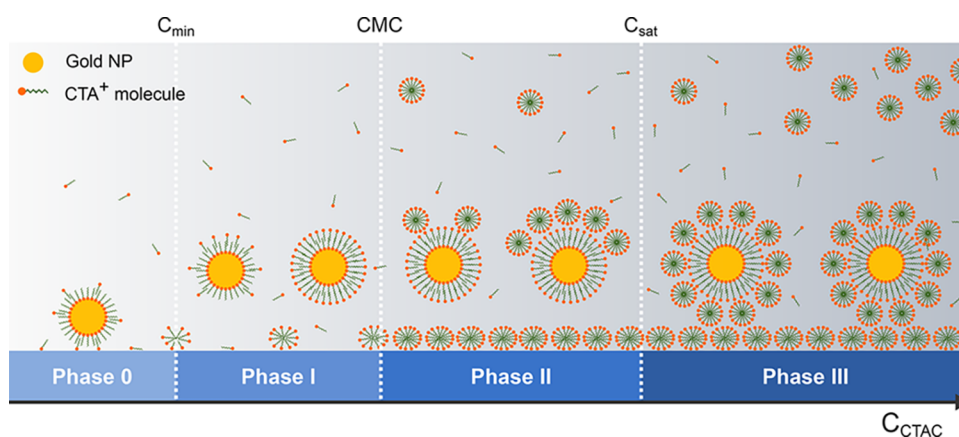


Figure 4. Cartoon showing plausible morphologies of adsorbed surfactant cations, CTA^+ , at the glass–water interface and the gold nanoparticles' surfaces at varying CTAC concentrations from low (left) to high (right). Adapted from Li et al.⁴⁷ for gold colloid surfaces and Tyrode et al.⁴⁶ for a glass–water interface.

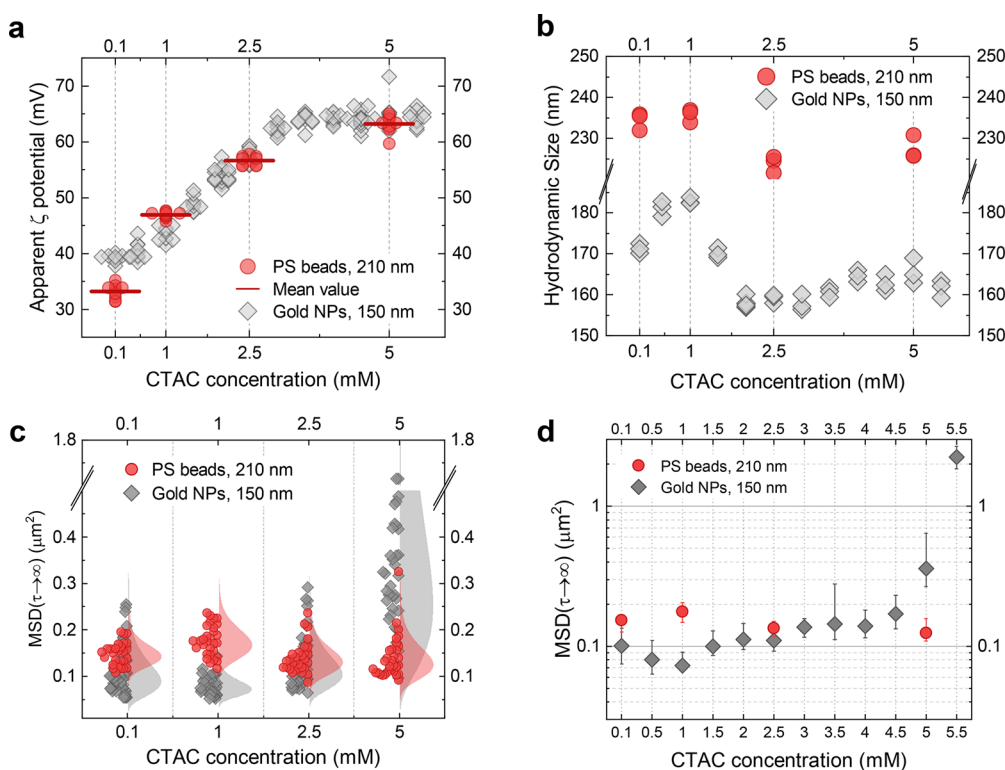


Figure 5. Polystyrene (PS) beads as a nonthermal probe. (a) Zeta potential and (b) hydrodynamic size of the PS beads compared with those of gold nanoparticles as a function of CTAC concentration. Each data point represents an average of 10 measurements. For each concentration, 10 data points are displayed for the ζ potential, and 3 data points are displayed for the hydrodynamic size. (c) Distributions of $\text{MSD}(\tau \rightarrow \infty)$ for optically trapped PS beads near the glass wall. The left half shows the data points of at least 30 measurements, and the right half shows the fitted log-normal distribution. The data and its distribution for gold nanoparticles are plotted behind for comparison. (d) Comparison of the $\text{MSD}(\infty)$ between gold and PS nanoparticles for the whole concentration range in semilogarithmic scale. The data points represent the mode of each distributions. The error bars indicate the $\langle 25,75\% \rangle$ interquartile range.

Figure 4 summarizes plausible morphologies of adsorbed surfactant molecules on the glass substrate and gold colloids, at increasing CTAC concentrations (see [Supplementary Video 1](#) for corresponding particle recordings). It depicts gradual changes in the surface coverage as well as the likely surfactant assemblies on different interfaces, adapted from Li et al.⁴⁷ and Tyrode et al.⁴⁶ Below the lowest concentration (C_{\min}), the particle is electrostatically attracted and stuck on the negatively charged glass surface (Phase 0). For stable colloids, a minimum concentration of 0.1 mM was required in this study. From C_{\min}

to CMC (Phase I), the particle trapped close to the glass wall may rearrange the admicelles, inducing a self-constraint on its movement and thus exhibiting the most stable trapping among the examined concentration groups. From CMC up to C_{sat} (Phase II), the particle is stably trapped on the fully covered glass surface, where the effect of the admicelles vanishes. At this stage, the particle surface has not yet been saturated. Above C_{sat} (Phase III), all the interfaces are completely saturated, and the particle starts to be impeded while finding a stable trap position, possibly due to the effect of the surfactants in the bulk.^{23,25}

Polystyrene Beads. We explained the motion of the trapped gold nanoparticles based on the surfactant assembly structures that develop with increasing surfactant concentration (admicelles, bilayers, and micelles in the bulk) and the possible influence of the particle on these structures. One of the hypotheses was the thermal effect of the optically trapped gold nanoparticles, which causes the local rearrangement of admicelles at the glass–solution interface. To test this hypothesis, we performed trapping experiments with polystyrene (PS) beads, which absorb much less light and thus produce much less heat (Supporting Information Figure S3 for the absorbance spectrum for gold and PS nanoparticles).

We used PS beads that have carboxyl groups on their surfaces, making them negatively charged (-41.5 ± 0.5 mV) like the gold nanoparticles with citrate coatings (-27.2 ± 0.2 mV). Figure 5a,b show their ζ potentials and hydrodynamic sizes as a function of CTAC concentration, superimposed on the gold nanoparticle data for comparison. The initially negative surface charge became immediately positive with the addition of CTA⁺ molecules, and their ζ potential magnitudes changed almost identically to those of gold nanoparticles with increasing CTAC concentration (Figure 5a). The development of their hydrodynamic size also resembles those of gold nanoparticles with about 70 nm offset (Figure 5b). The similar behaviors in the surface charges and the stark contrast in the optical absorbance make the PS beads a successful candidate to test the thermal effects.

Figure 5c summarizes the MSD analysis for the PS beads, with the results for gold nanoparticles for comparison. The beads were trapped by the same optical tweezer at four different CTAC concentrations (0.1, 1, 2.5, and 5 mM). By comparing the results from this nonthermal probe, we discovered a few interesting differences. First, the distributions remain similar across vastly different concentrations, supporting our hypothesis that the changes originate from the thermal effects. Furthermore, the distributions for the PS beads are narrower and symmetrical. We have previously explained the gold nanoparticles' skewed distribution by combining the asymmetric size distribution and size-dependent optical heating. The PS beads also have an asymmetric log-normal size distribution with a comparable variance (Supporting Information Figure S4a), but the optical heating effects are absent in this case. Therefore, we can understand that the optical heating makes the distribution skewed and broader for gold nanoparticles. The remaining variance in the MSD(∞) distribution for the PS beads can be attributed to other experimental variations such as the surface charges and shapes of the particles and site-specific local surface variations. The only exception occurs at 1.0 mM CTAC, where the gold nanoparticles have a narrower yet skewed distribution. As we suggested earlier, it may be explained by the interactions with the admicelles, which disrupt the distribution of admicelles and reduce their randomness through rearrangement.

Figure 5d reveals the different developments of the MSD(∞) for the gold and PS nanoparticles. The points and error bars respectively represent the modes and interquartile ranges (25–75%) of the data. The modes of the PS beads remain similar, as expected from Figure 5c, showing neither the decrease in Phase I nor the increase in Phase III that are observed for the gold nanoparticles. The overall shifts of the MSDs to higher values for the PS beads can be attributed to weak axial confinement due to their relatively small scattering force compared to that of the highly reflective gold nanoparticles. Since the ζ potential of the PS beads and the surface coverage of the glass substrate

drastically change over the examined concentration range, the adsorption of surfactant molecules seems to have negligible effects on the motion of the PS particles. It also appears that the micelles in bulk do not perturb the trap from the results at 5.0 mM CTAC. Therefore, the observations with the PS beads support the two hypotheses regarding the thermal effects of the gold nanoparticles on their motions, namely the heat-induced migration of the adsorbed micelles on the glass surface at low concentrations and the disturbance caused by the bulk micelles in the presence of a temperature gradient at high concentrations.

CONCLUSION

This paper has studied the effect of adsorbed surfactants (CTAC) on an optically trapped gold nanoparticle by analyzing its trajectories inside the trap. Close to the liquid–glass interface, the particle interacts with the surfactants in a way that strengthens or inversely disturbs stable trapping, depending on the surfactant concentration. Below the CMC, we have evidenced that the unsaturated surfactant layer can create an additional trapping potential. The interaction between the surfactant admicelles and the optical heated metallic particle has been suggested as a possible mechanism, which was supported by theoretical modeling using the DLVO theory and controlled experiments with cooler PS beads. Above the concentration at which both the particle and glass surfaces are fully saturated, we have found that micelles in bulk perturb the optical trap, analogous to the recent findings by Lin et al.²³ Our findings develop a fundamental understanding of the influence of surfactants on optically trapped objects, where surfactants are often required for colloidal stability. The same methodology can be applied to different combinations of surfactants, colloidal particles, and substrates. Moreover, a gold nanoparticle as a thermal probe can become a versatile tool in surface sciences to locally elevate the temperature around the particle and simultaneously investigate temperature-related phenomena such as desorption or polymerization, by statistically analyzing its motion.

ASSOCIATED CONTENT

Supporting Information

The Supporting Information is available free of charge at <https://pubs.acs.org/doi/10.1021/acs.jpcc.1c08975>.

Overview of the optical setup; ζ measurements at different particle concentrations; absorbance spectrum of gold colloids and PS beads; size distributions measured by dynamic light scattering and the Mie absorption calculated for the measured size range; hydrodynamic drags estimated from MSD data fitting; calculation of interaction force between admicelles and trapped particles using the DLVO theory (PDF)

Supplementary video 1: Compilation of separate recordings for optically trapped particles at three different CTAC concentrations (1, 2.5, and 5.5 mM), presented together with the recording of a stuck particle for reference (MP4)

AUTHOR INFORMATION

Corresponding Author

Olivier J. F. Martin – Nanophotonics and Metrology
Laboratory, Swiss Federal Institute of Technology Lausanne (EPFL), 1015 Lausanne, Switzerland; orcid.org/0000-

0002-9574-3119; Phone: +41 (0)21 693 2607;
Email: olivier.martin@epfl.ch

Author

Jeonghyeon Kim – Nanophotonics and Metrology Laboratory,
Swiss Federal Institute of Technology Lausanne (EPFL), 1015
Lausanne, Switzerland; orcid.org/0000-0002-7018-9211

Complete contact information is available at:
<https://pubs.acs.org/10.1021/acs.jpcc.1c08975>

Notes

The authors declare no competing financial interest.

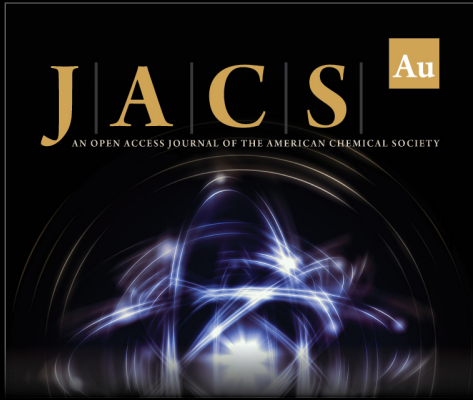
ACKNOWLEDGMENTS

Funding from the European Research Council (ERC-2015-AdG-695206 Nanofactory) is gratefully acknowledged.

REFERENCES


- (1) Ashkin, A. Acceleration and Trapping of Particles by Radiation Pressure. *Phys. Rev. Lett.* **1970**, *24*, 156–159.
- (2) Ashkin, A.; Dziedzic, J. M. Optical Levitation by Radiation Pressure. *Appl. Phys. Lett.* **1971**, *19*, 283–285.
- (3) Ashkin, A. Applications of Laser Radiation Pressure. *Science* **1980**, *210*, 1081–1088.
- (4) Ashkin, A.; Dziedzic, J. M.; Bjorkholm, J. E.; Chu, S. Observation of a Single-Beam Gradient Force Optical Trap for Dielectric Particles. *Opt. Lett.* **1986**, *11*, 288–290.
- (5) Grier, D. G. A Revolution in Optical Manipulation. *Nature* **2003**, *424*, 810–816.
- (6) Bowman, R. W.; Padgett, M. J. Optical Trapping and Binding. *Rep. Prog. Phys.* **2013**, *76*, 026401.
- (7) Maragò, O. M.; Jones, P. H.; Gucciardi, P. G.; Volpe, G.; Ferrari, A. C. Optical Trapping and Manipulation of Nanostructures. *Nat. Nanotechnol.* **2013**, *8*, 807.
- (8) Ashkin, A.; Dziedzic, J. M. Optical Trapping and Manipulation of Viruses and Bacteria. *Science* **1987**, *235*, 1517–1520.
- (9) Min, T. L.; Mears, P. J.; Chubiz, L. M.; Rao, C. V.; Golding, I.; Chemla, Y. R. High-Resolution, Long-Term Characterization of Bacterial Motility Using Optical Tweezers. *Nat. Methods* **2009**, *6*, 831–835.
- (10) Pang, Y.; Song, H.; Kim, J. H.; Hou, X.; Cheng, W. Optical Trapping of Individual Human Immunodeficiency Viruses in Culture Fluid Reveals Heterogeneity With Single-Molecule Resolution. *Nat. Nanotechnol.* **2014**, *9*, 624–630.
- (11) Svoboda, K.; Schmidt, C. F.; Schnapp, B. J.; Block, S. M. Direct Observation of Kinesin Stepping by Optical Trapping Interferometry. *Nature* **1993**, *365*, 721–727.
- (12) Molloy, J. E.; Burns, J. E.; Kendrick-Jones, J.; Tregear, R. T.; White, D. C. S. Movement and Force Produced by a Single Myosin Head. *Nature* **1995**, *378*, 209–212.
- (13) Grier, D. G. Optical Tweezers in Colloid and Interface Science. *Curr. Opin. Colloid Interface Sci.* **1997**, *2*, 264–270.
- (14) Polin, M.; Grier, D. G.; Quake, S. R. Anomalous Vibrational Dispersion in Holographically Trapped Colloidal Arrays. *Phys. Rev. Lett.* **2006**, *96*, 088101.
- (15) Franosch, T.; Grimm, M.; Belushkin, M.; Mor, F. M.; Foffi, G.; Forró, L.; Jeney, S. Resonances Arising From Hydrodynamic Memory in Brownian Motion. *Nature* **2011**, *478*, 85–88.
- (16) McCann, L. I.; Dykman, M.; Golding, B. Thermally Activated Transitions in a Bistable Three-Dimensional Optical Trap. *Nature* **1999**, *402*, 785–787.
- (17) Carberry, D. M.; Reid, J. C.; Wang, G. M.; Sevick, E. M.; Searles, D. J.; Evans, D. J. Fluctuations and Irreversibility: An Experimental Demonstration of a Second-Law-Like Theorem Using a Colloidal Particle Held in an Optical Trap. *Phys. Rev. Lett.* **2004**, *92*, 140601.
- (18) Bérut, A.; Arakelyan, A.; Petrosyan, A.; Ciliberto, S.; Dillenschneider, R.; Lutz, E. Experimental Verification of Landauer's Principle Linking Information and Thermodynamics. *Nature* **2012**, *483*, 187–189.
- (19) Yao, A.; Tassieri, M.; Padgett, M.; Cooper, J. Microrheology with Optical Tweezers. *Lab Chip* **2009**, *9*, 2568–2575.
- (20) Neuman, K. C.; Block, S. M. Optical Trapping. *Rev. Sci. Instrum.* **2004**, *75*, 2787–2809.
- (21) Tadros, T. General Principles of Colloid Stability and the Role of Surface Forces. *Colloid Stability* **2014**, 1–22.
- (22) Shrestha, S.; Wang, B.; Dutta, P. Nanoparticle Processing: Understanding and Controlling Aggregation. *Adv. Colloid Interface Sci.* **2020**, *279*, 102162.
- (23) Lin, L.; Wang, M.; Peng, X.; Lissek, E. N.; Mao, Z.; Scarabelli, L.; Adkins, E.; Coskun, S.; Unalan, H. E.; Korgel, B. A.; et al. Opto-Thermoelectric Nanotweezers. *Nat. Photonics* **2018**, *12*, 195–201.
- (24) Liu, Y.; Lin, L.; Bangalore Rajeeva, B.; Jarrett, J. W.; Li, X.; Peng, X.; Kollipara, P.; Yao, K.; Akinwande, D.; Dunn, A. K.; et al. Nanoradiator-Mediated Deterministic Opto-Thermoelectric Manipulation. *ACS Nano* **2018**, *12*, 10383–10392.
- (25) Jiang, Q.; Rogez, B.; Claude, J.-B.; Baffou, G.; Wenger, J. Quantifying the Role of the Surfactant and the Thermophoretic Force in Plasmonic Nano-optical Trapping. *Nano Lett.* **2020**, *20*, 8811–8817.
- (26) Crocker, J. C.; Grier, D. G. Methods of Digital Video Microscopy for Colloidal Studies. *J. Colloid Interface Sci.* **1996**, *179*, 298–310.
- (27) Gibson, G. M.; Leach, J.; Keen, S.; Wright, A. J.; Padgett, M. J. Measuring the Accuracy of Particle Position and Force in Optical Tweezers Using High-Speed Video Microscopy. *Opt. Express* **2008**, *16*, 14561–14570.
- (28) Otto, O.; Gornall, J. L.; Stober, G.; Czerwinski, F.; Seidel, R.; Keyser, U. F. High-Speed Video-Based Tracking of Optically Trapped Colloids. *J. Opt.* **2011**, *13*, 044011.
- (29) Jain, P. K.; Lee, K. S.; El-Sayed, I. H.; El-Sayed, M. A. Calculated Absorption and Scattering Properties of Gold Nanoparticles of Different Size, Shape, and Composition: Applications in Biological Imaging and Biomedicine. *J. Phys. Chem. B* **2006**, *110*, 7238–7248.
- (30) Maier, S. *Plasmonics: Fundamentals and Applications*; Springer: New York, 2007.
- (31) Baffou, G.; Girard, C.; Quidant, R. Mapping Heat Origin in Plasmonic Structures. *Phys. Rev. Lett.* **2010**, *104*, 136805.
- (32) Baffou, G.; Quidant, R. Thermo-Plasmonics: Using Metallic Nanostructures as Nano-Sources of Heat. *Laser Photonics Rev.* **2013**, *7*, 171–187.
- (33) Baffou, G.; Cichos, F.; Quidant, R. Applications and Challenges of Thermoplasmonics. *Nat. Mater.* **2020**, *19*, 946–958.
- (34) Zhang, W.; Huang, L.; Santschi, C.; Martin, O. J. F. Trapping and Sensing 10 nm Metal Nanoparticles Using Plasmonic Dipole Antennas. *Nano Lett.* **2010**, *10*, 1006–1011.
- (35) Allan, D. B.; Caswell, T.; Keim, N. C.; van der Wel, C. M.; Verweij, R. *soft-matter/trackpy: Trackpy v0.5.0*, 2021; https://zenodo.org/record/4682814#_YcC2k2jMLIU (accessed 1 September 2021).
- (36) Kim, J.; Martin, J. F. O. *Dataset for the Manuscript: Surfactants Control Optical Trapping Near a Glass Wall*, 2021; https://zenodo.org/record/5557074#_YcC2_2jMLIU.
- (37) Nørrelykke, S. F.; Flyvbjerg, H. Harmonic Oscillator in Heat Bath: Exact Simulation of Time-Lapse-Recorded Data and Exact Analytical Benchmark Statistics. *Phys. Rev. E* **2011**, *83*, 041103.
- (38) Bendix, P. M.; Reihani, S. N. S.; Oddershede, L. B. Direct Measurements of Heating by Electromagnetically Trapped Gold Nanoparticles on Supported Lipid Bilayers. *ACS Nano* **2010**, *4*, 2256–2262.
- (39) Kyrsting, A.; Bendix, P. M.; Stamou, D. G.; Oddershede, L. B. Heat Profiling of Three-Dimensionally Optically Trapped Gold Nanoparticles using Vesicle Cargo Release. *Nano Lett.* **2011**, *11*, 888–892.
- (40) Lemons, D. S.; Gythiel, A. Paul Langevin's 1908 paper "On the Theory of Brownian Motion" ["Sur la théorie du mouvement brownien," C. R. Acad. Sci. (Paris) **146**, 530–533 (1908)]. *Am. J. Phys.* **1997**, *65*, 1079–1081.


- (41) Purcell, E. M. Life at Low Reynolds Number. *Am. J. Phys.* **1977**, *45*, 3–11.
- (42) Nikoobakht, B.; El-Sayed, M. A. Evidence for Bilayer Assembly of Cationic Surfactants on the Surface of Gold Nanorods. *Langmuir* **2001**, *17*, 6368–6374.
- (43) Liu, J.-F.; Min, G.; Ducker, W. A. AFM Study of Adsorption of Cationic Surfactants and Cationic Polyelectrolytes at the Silica-Water Interface. *Langmuir* **2001**, *17*, 4895–4903.
- (44) Atkin, R.; Craig, V.; Wanless, E.; Biggs, S. Mechanism of Cationic Surfactant Adsorption at the Solid–Aqueous Interface. *Adv. Colloid Interface Sci.* **2003**, *103*, 219–304.
- (45) Gao, Y.; Du, J.; Gu, T. Hemimicelle Formation of Cationic Surfactants at The Silica Gel–Water Interface. *J. Chem. Soc., Faraday Trans. 1* **1987**, *83*, 2671–2679.
- (46) Tyrode, E.; Rutland, M. W.; Bain, C. D. Adsorption of CTAB on Hydrophilic Silica Studied by Linear and Nonlinear Optical Spectroscopy. *J. Am. Chem. Soc.* **2008**, *130*, 17434–17445.
- (47) Li, R.; Wang, Z.; Gu, X.; Chen, C.; Zhang, Y.; Hu, D. Study on the Assembly Structure Variation of Cetyltrimethylammonium Bromide on the Surface of Gold Nanoparticles. *ACS Omega* **2020**, *5*, 4943–4952.
- (48) Reiss-Husson, F.; Luzzati, V. The Structure of the Micellar Solutions of Some Amphiphilic Compounds in Pure Water as Determined by Absolute Small-Angle X-Ray Scattering Techniques. *J. Phys. Chem.* **1964**, *68*, 3504–3511.
- (49) Williams, R. J.; Phillips, J. N.; Mysels, K. J. The Critical Micelle Concentration of Sodium Lauryl Sulphate at 25 °C. *Trans. Faraday Soc.* **1955**, *51*, 728–737.
- (50) Pérez-Rodríguez, M.; Prieto, G.; Rega, C.; Varela, L. M.; Sarmiento, F.; Mosquera, V. A Comparative Study of the Determination of the Critical Micelle Concentration by Conductivity and Dielectric Constant Measurements. *Langmuir* **1998**, *14*, 4422–4426.
- (51) Tofani, L.; Feis, A.; Snoke, R. E.; Berti, D.; Baglioni, P.; Smulevich, G. Spectroscopic and Interfacial Properties of Myoglobin/Surfactant Complexes. *Biophys. J.* **2004**, *87*, 1186–1195.
- (52) Bijsterbosch, B. Characterization of Silica Surfaces by Adsorption From Solution. Investigations Into the Mechanism of Adsorption of Cationic Surfactants. *J. Colloid Interface Sci.* **1974**, *47*, 186–198.
- (53) Schäffer, E.; Nørrelykke, S. F.; Howard, J. Surface Forces and Drag Coefficients of Microspheres near a Plane Surface Measured with Optical Tweezers. *Langmuir* **2007**, *23*, 3654–3665.
- (54) Happel, J.; Brenner, H. *Low Reynolds number hydrodynamics: with special applications to particulate media*; Springer: Dordrecht, 1983; Vol. 1.
- (55) Seol, Y.; Carpenter, A. E.; Perkins, T. T. Gold Nanoparticles: Enhanced Optical Trapping and Sensitivity Coupled With Significant Heating. *Opt. Lett.* **2006**, *31*, 2429–2431.
- (56) Atkins, P.; De Paula, J. *Atkins' Physical Chemistry*, 10th ed.; Oxford University Press: Oxford, UK, 2014; Chapter 14, pp 628–629.



JACS Au
AN OPEN ACCESS JOURNAL OF THE AMERICAN CHEMICAL SOCIETY

Editor-in-Chief
Prof. Christopher W. Jones
Georgia Institute of Technology, USA

Open for Submissions 

pubs.acs.org/jacsau  ACS Publications
Most Trusted. Most Cited. Most Read.